Testing and performances of Spectroscopic Radiation Portal Monitor for homeland security

C. Deyglun, IRSN

—Each year States report to IAEA loss, theft or out of regulatory control radioactive materials. Most incidents are minor, but material is potentially available for criminal acts. Measures to reduce the radiological and nuclear threat are many-faceted. An important component is the ability to detect illicit transport of radioactive material. Spectroscopic Radiation Portal Monitors are deployed around the world to detect illegal radioactive material traffic. A combination of experimental data collected during testing campaigns and simulations is a good way to study the performance of Spectroscopic Radiation Portal Monitors in realistic conditions. The paper presents a process to evaluate the performances of a portal, based on a combination of experimental data and MCNP simulations to calculate the detection probability and the false alarm rate. IRSN developed platforms for testing Spectroscopic Radiation Portal Monitors for pedestrian control. Experimental data were collected from an available commercial Spectroscopic Radiation Portal Monitor, tested in the framework of the Illicit Trafficking Radiation Assessment Program phase II Round Robin Test. Many scenarios were tested with different sources using realistic setups and many experimental data were collected. The tested equipment was then simulated with MCNP only based on the data provided in the user manual and the standards found in the industry. To get a realistic idea of the uncertainty, all the variables inherent in the measurement were considered, their relative contributions were identified and quantified, then propagated to predict an overall uncertainty. The combination of experimental data, numerical simulations and uncertainty evaluation showed good agreement with experimental assays. The results were used to test the sensitivity of a Spectroscopic Radiation Portal Monitor to special nuclear materials for different alarm thresholds. This process applied to different scenarios according to defined targets should help in the selection of operating characteristics of the portal.

***Keyword* — Safeguards, Homeland security, Nuclear security, Gamma-ray detection, Radioactive source detection**

I. Introduction

In recent years, the threat of nuclear and radiological terrorism have raised at the international level [1]. A significant number of incidents of trafficking of nuclear materials have been recorded in the IAEA Incident and Trafficking Database [2]. For example, in 2013 incident reported by the IAEA [3] included details of a group of traffickers convicted in Moldova for attempting to sell quantities of uranium and plutonium that had been transported in shielded lead canisters in an attempt to lure detection systems. Measures to reduce the radiological and nuclear threat are many-faceted. An important component is the ability to detect illicit transport of radioactive material. Spectroscopic Radiation Portal Monitors (SRPM) are deployed at front-line sites around the world to detect illegal radioactive material traffic. The Illicit Trafficking Radiation Assessment Program (ITRAP+10) is a program initiated by the European Union and the United States [4, 5]. From 2011 to 2016, the first phase aimed at evaluating the performance of available commercial radiation detection equipment against the American National Standards Institute/Institute of Electrical and Electronics Engineers (ANSI/IEEE) and the International Electrotechnical Commission (IEC) published consensus standards. During the second phase (ITRAP+10 phase II Round Robin Test), started in 2017, an available commercial Spectroscopic Radiation Portal Monitor was tested by five European laboratories including IRSN. For this purpose, IRSN developed testing platforms and collected experimental data. In parallel, a MCNP model of the portal was developed based on the data provided in the user manual and the standards found in the industry in order to study the sensitivity of such portal to special nuclear materials. The paper presents an evaluation of the performances of a SRPM based on few experimental data and simulations. At first the tested SRPM is simulated with MCNP6 [6] and it's response to point sources is compared to experimental results to adjust the model. Then based on such model, the response to HEU source is simulated and uncertainties are calculated. Finally the Detection probability is calculated through simulations.

C. Deyglun works for the Institute for Radiological Protection and Nuclear Safety, Fontenay-aux-Roses, BP 17 - 92 262, France (e-mail: clement.deyglun@ irsn.fr).

II. Performance Evaluation By Simulation

.

A. Modelling the SRPM response

The SRPM is based on inorganic scintillator NaI(Tl) to detect gamma-rays. The energy resolution of the full energy peak of a scintillator coupled to a photomultiplier tube depends on the intrinsic resolution of the crystal and the photomultiplier tube contribution. The Full Width at Half Maximum (FWHM) curve according to gamma-rays energy is expressed by the following function:

$$FWHM = a + b\sqrt{E + cE^2} \quad (1)$$

Where E is incident gamma rays energy (MeV) and a, b, c are

constants from the fitting function. A set of measurements with Am-241, Cs-137, Co-60 and Eu-152 sources were performed (see Fig. 1) in order to determine the energy resolution, and the curve's coefficients were introduced in the function provided by the GEB command of MCNP6 code that fits a Gaussian to the spectrum to make the proper corrections.

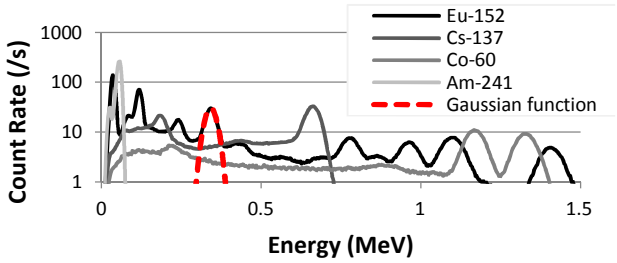

Fig 1. Gamma spectra fitting with a Gaussian function.

The SRPM model was developed based on the data of the user manual (for example: mechanical parts, shields, detectors dimensions), the standards found in the industry (e.g. NaI(Tl) crystals are generally machined and mounted in a housing of aluminum with standard thickness of 0.5 mm) and some simple assumptions (for example: the presence of a photomultiplier and electronic component inside the SRPM). Different model of the SRPM were tested, the first one is only composed of the NaI(Tl) bloc, the second is composed of the NaI(Tl) bloc and structure of the portal, and the last model is composed of the complete SRPM and its surroundings. These models allow estimating the best compromise between the complexity of the model and a good agreement with experimental measurement. They are presented in Fig. 2

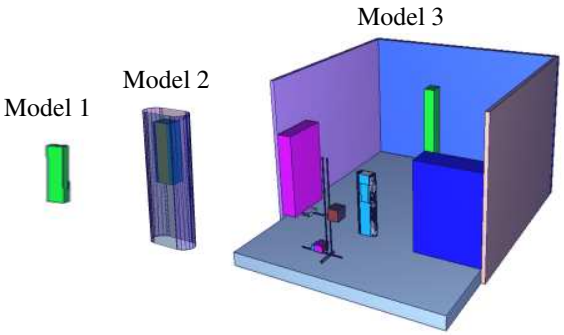

Fig.2. Tested models of the SRPM.

A pulse height distribution estimate (F8 tally), was used to obtain the deposited energy distribution per incident photon in the detector volume. A comparison between empirical spectrum and MCNP6 simulated spectra of the NaI(Tl) detector in the case of a Eu-152 source is shown in Fig. 3.

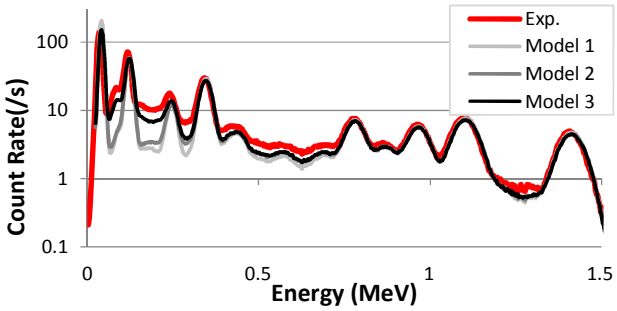

Fig 3. Comparison between experimental and simulated pulse height distributions of a Eu-152 source.

A good agreement between simulated and measured energy spectra can be seen. While for the high-energy gamma rays the measured and calculated spectra match well, for the low-energy gamma-rays however a systematic difference and an under-estimation of the models are observed. The first one is due to non-proportional scintillation efficiency of the NaI(Tl) crystals at low energy region [7]. The scintillation efficiency is defined as the light output per unit deposited energy, is not a constant value and is not considered in MCNP6 simulation. The second is due to the bad simulation of peaks arising from Compton scattering of gamma rays in the room's walls and in the shield surrounding the detector. The results presented in Fig. 3 indicate that:

- A complete setup model is important at low energy;
- The data of the user manual and basic knowledge about the composition of the SRPM are enough to obtain good agreement between simulated and experimental spectra;
- There is a good agreement for medium and high energy peaks;
- Gamma rays from Compton scattering of gamma rays in the surrounding environment are difficult to model.

B. Alarm Threshold Calculation

False-alarms are caused by statistical variations in background counting. In a defined region of spectra (Region Of Interest: ROI), count varies according to a Poisson distribution, with a standard deviation, which is the root square of the number of counts. The alarm threshold (AL) is a compromise between sensitivity and the false alarms. AL can be expressed as a distance above the mean background (BKG) value in terms of standard deviation:

$$AL = BKG + M\sqrt{BKG} \quad (2)$$

M is a multiple that provides a constant false-alarm rate at any background intensity. The probability for one acquisition without radioactive source to exceed AL (i.e. the false alarm probability) is presented in TABLE I.

TABLE I
PROBABILITY OF EXCEEDING THE ALARM THRESHOLD AL [8]

Multiplier M	False alarm probability per acquisition
0	0.5
1	0.1586
2	2.275×10^{-2}
3	1.35×10^{-3}
4	3.15×10^{-5}
5	2.85×10^{-7}

The Alarm is triggered if the dose rate excesses the dose rate threshold or if the number of counts inside one Region of Interet of the spectrum (ROI 1 30 keV – 300 keV, ROI 2 300 keV-800 keV, and ROI 3 800 keV – 3000 keV) raises the threshold AL. The paper only focuses on the detection through the counting inside ROIs.

C. Model a static source

Based on model 3, many sources were tested with a static platform presented in Fig. 4, with 2 s per acquisition (see spectrum in Fig. 5, 6 and 7). In order to take into account the ambient background radiations, the experimental spectrum of background is added in the simulated spectrum.

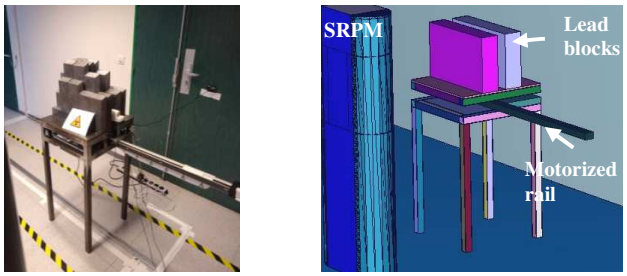

Fig. 4 Static platform (on the left : experimental setup, on the right model).

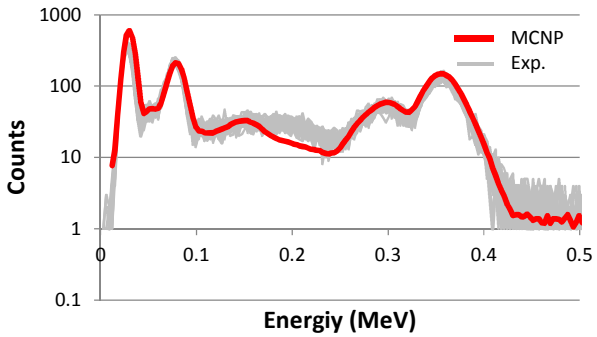

Fig.5. *Comparison between 30 experimental and one simulated pulse height distributions from a Ba-133 source for 2s acquisition time.*

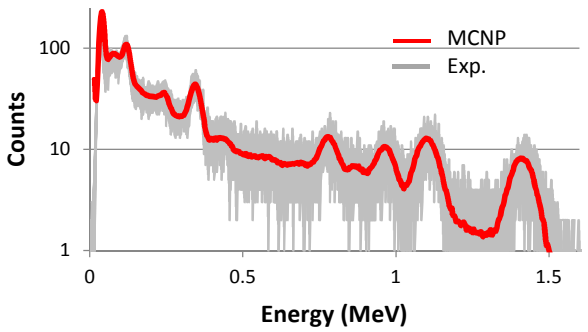

Fig.6. Comparison between 30 experimental and one simulated pulse height distributions from a Eu-152 source inside PEHD container (thick 8 cm) for 2s acquisition time.

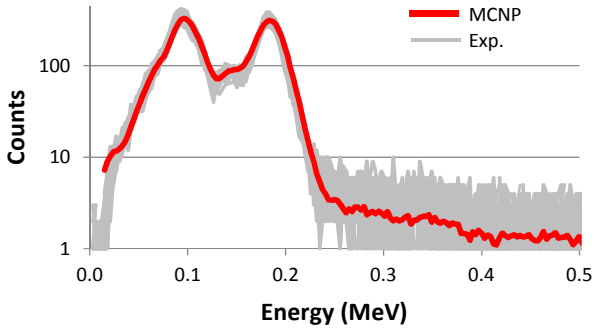

Fig.7. Comparison between 30 experimental and one simulated pulse height distributions from HEU source for 2s acquisition time.

TABLE II summarizes the comparison between experimental and simulated measurements for the three tested sources.

TABLE II
COMPARAISON BETWEEN EXPERIMENTZL AND SIMULATED RESULTS $MS\frac{im\,ul.}{Exp}\frac{xp.}{-E}$

ROI	**HEU**	**Eu-152**	**Ba-133**
ROI 1 [30 keV - 300 keV[	4.12%	20.66%	17.47%
ROI 2 [300 keV - 800 keV[	14,75%	3.41%	13.29%
ROI 3 [800 keV - 3000 keV]	6.82%	7.43%	4.61%

HEU does not have high energy gamma-rays, so the difficult-to-simulate continuum Compton is low and there are no very low energy gamma-rays which are very sensitive to attenuation simulation. Therefore there is a good agreement between experimental and simulated spectra in in ROI1.

1) Uncertainties

To get a realistic idea of the measurement uncertainty, all the variables inherent to the measurement were considered,

their uncertainties were identified and quantified, and they were propagated to predict an overall uncertainty. The paragraph focuses on the detection of HEU source.

a) Location uncertainty

The position of the source has a significant impact on the results. An area of "possible locations" is defined in Fig. 8. It corresponds to the middle of an "average" human body, the bottom of this legs and the top of the torso.

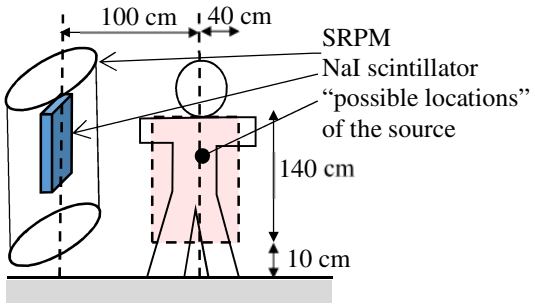

Fig. 8. Source locations.

It was assumed that the HEU source could be uniformly moved within the area described in Fig. 8. These locations are simulated in Fig. 9 to calculate its impact and counts in ROI 1 distribution is presented in Fig. 10.

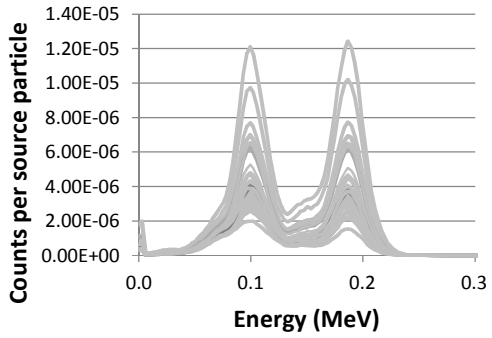

Fig.9. Simulation of the impact of the source's location on spectra (31 spectra).

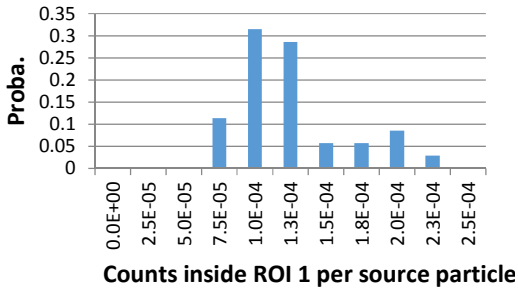

Fig. 10. Distribution of the counts in ROI 1 for HEU source simulation.

In the case of the HEU source, most of the gamma-rays are emitted below 300 keV. Hence, only ROI 1 is relevant. The variance distribution of the counts inside ROI 1 gives the uncertainty $\sigma_{Loca.}(ROI_1)$ and the relative uncertainty $\sigma_{Loca.\ Relat.}(ROI_1) = 46.4\%$.

The uncertainty related to source location is the main contributor to the useful signal of the radioactive source. The useful signal U can be expressed as follows:

$$U = U_0 + CF_{Location} \tag{3}$$

Where U_0 is the signal induced by the source at reference location (in the study 100 cm away from the center of the detector and 100 cm height) and $CF_{Location}$ is a correction factor which depends on the source location. The uncertainty related to the source location can be expressed as follows:

$$\sigma_{U\ Relat.} = \sqrt{{\sigma_{stat}}^2 + {\sigma_{Loca.Relat.}}^2} \tag{4}$$

b) Background uncertainty

As presented in Equation 2, detection efficiency of the SRPM is influenced by the background radiation and variation of its intensity with time. Variations in background intensity can be caused by people walk-trough, natural background radiation process or movement of radioactive materials. The last one is ignored; in the study it is supposed a perfect control of the radioactive materials in the vicinity of the SRPM area.

During the crossing through the SRPM detection area, the pedestrian partly absorbs the ambient background radiations and decreases the measured background. For example a truck in the detection area of a vehicle monitor reduces the measured background from 10% to 25% [9]. Because the monitor's alarm threshold is defined before the presence of an occupant, background decrease is not taken into account and a much larger signal is required to alarm an occupied monitor than an unoccupied one.

To estimate the impact of people walk-through, several acquisitions were performed, with and without a polyethylene phantom in the detection area of the SRPM (see Fig. 11). The variation in intensity has been calculated in the three ROIs. Assuming a uniform distribution of the variation between the minimum (BKG_{min}) and maximum (BKG_{max}) measured background, the background uncertainty is given by the following formula:

$$\sigma = (BKG_{max} - BKG_{min})/2\sqrt{3} \tag{5}$$

The background uncertainty is estimated within the three ROIs:

$\sigma^{Occupant}_{BKG\ relat.}(ROI_1) = 0.0030\%$
$\sigma^{Occupant}_{BKG\ relat.}(ROI_2) = 0.0021\%$
$\sigma^{Occupant}_{BKG\ relat.}(ROI_1) = 0.0015\%$

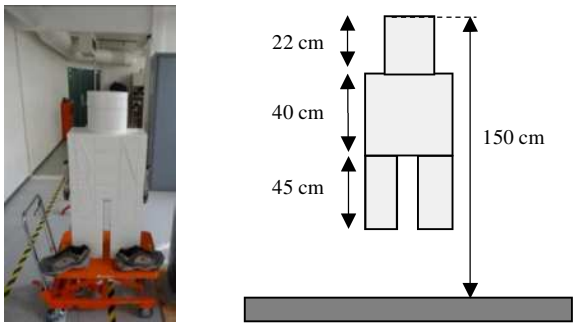

Fig. 11. Polyethylene phantom in the detection area.

The natural background radiation originates from a variety of sources, cosmic radiation and environmental radioactivity from naturally occurring radioactive materials (such as radon and radium). It varies with location and time. Many short background acquisitions (122 s) were done with "stable" environmental conditions (temperature, atmospheric pressure and humidity) in Fig. 12.

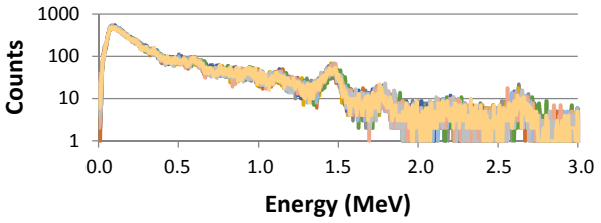

Fig. 12. Background spectra for 122s acquisitions.

The variance distribution of the counts inside ROI 1, 2 and 3 is estimated:

$\sigma_{BKG\ relat.}^{Natural}(ROI_i) = 1.89\%$
$\sigma_{BKG\ relat.}^{Natural}(ROI_2) = 1.92\%$
$\sigma_{BKG\ relat.}^{Natural}(ROI_3) = 1.42\%.$

The total background uncertainty is calculated based on these two contributions, people walk-trough and natural variations. Within each ROI i (i=1, 2, 3), the background contribution can be expressed as the sum of a "stable" background $BKG_0(ROI_i)$, variation due to people walk-trough $\Delta_{Occupant}(ROI_i)$ and natural variation $\Delta_{Natural}(ROI_i)$:

$$BKG(ROI_i) = BKG_0(ROI_i) + \Delta_{Occupant}(ROI_i) + \Delta_{Natural}(ROI_i) \quad (6)$$

Hence background uncertainty is expressed as follows:

$$\sigma_{BKG}(ROI_i) = \sqrt{\sigma_{BKG}^{statistic}(ROI_i)^2 + \sigma_{BKG}^{Occupant}(ROI_i)^2 + \sigma_{BKG}^{sNatural}(ROI_i)^2} \quad (7)$$

Where $\sigma_{BKG}^{statistic}(ROI_i)$ is the statistical uncertainty.

c) Other sources of uncertainties

There are many other sources of uncertainties. For example, the internal absorption of gamma-rays depends on the material composition, density and shape. Thin uranium sample powders emit most of this radiation, whereas more compact shapes such as sphere are impacted by auto-absorption and absorb most of it [10]. The assumption "only one kind of nuclear material is available" is done in the study to neglect this contributor.

The presence of metallic shield, as modeled in Fig.13, is also an important uncertainty. It is assumed that iron shield and thick lead shield shall be detected by metallic detector portal. The impact of thin lead shield is simulated in Fig 14.

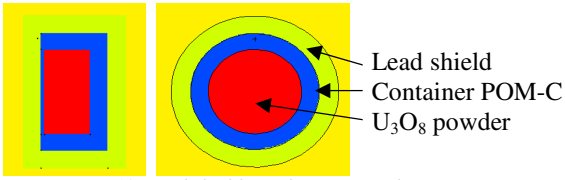

Fig. 13. Lead shield simulation around HEU source.

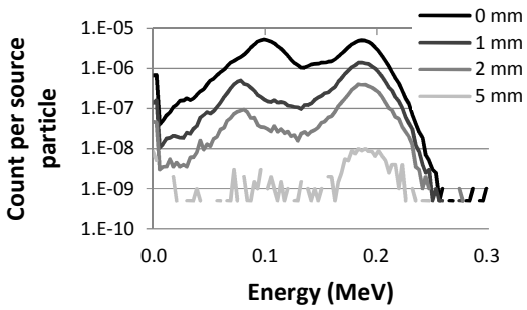

Fig. 14. Simulated spectra of shielded HEU sources.

Detection sensitivity is calculated for bare source and a correction factor is applied according to the scenario. For example if the signal from 1 bare source of 100g HEU is equivalent to 6 shielded 100g HEU sources wrapped by 1 mm lead. The shortcut "100g of HEU produces the same signal than 600g of 1mm lead shielded HEU" is not correct due to auto-absorption.

d) Conclusion about uncertainties

The measured signal S is the sum of the source signal (the useful signal U) and the background contribution BKG:

$$S = U + BKG \quad (8)$$

Therefore, the total uncertainty can be expressed as follows:

$$\sigma_S = \sqrt{{\sigma_U}^2 + {\sigma_{BKG}}^2} \quad (9)$$

Where σ_U and σ_{BKG} have been previously studied.

2) Detection probability

The coefficient M of the alarm threshold (see Equation 2) is fixed to limit false alarm rate and not disturb the flow of people through the SRPM. Fig. 15 illustrates the compromise between false-alarm rate and detection efficiency.

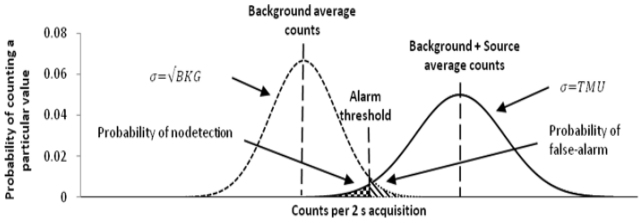

Fig. 15. Illustration of the background distribution and the distribution after addition of a source.

We assumed that the counting distribution from a SRPM is a Gaussian distribution:

$$P_{Measure}(c) = \frac{1}{\sigma\sqrt{2\pi}} exp\left(-\frac{(\bar{c}-c)^2}{2\sigma^2}\right) \quad (10)$$

Where $\bar{c}(m)$ is the average counts induced by m grams of HEU and σ the counting uncertainty. The detection probability is the area from $P_{Measure}$ above the alarm threshold AL, expressed as follows:

$$P_{Detection}(m) = \frac{1}{2} \times \left(1 - erf\left(\frac{AL-\bar{c}}{\sigma\sqrt{2}}\right)\right) \quad (11)$$

Where *erf* is the Gauss error function. To simplify calculations, in first approximation we neglect the variation of auto-absorption with the mass, a linear relation is assumed between the mass m of HEU and the average counts $\bar{c}(m)$ induced in the SRPM:

$$\bar{c}(m) = a \times m \quad (12)$$

Where the coefficient a is estimated with the MCNP model of the SRPM. Finally, the detection probability is calculated. Fig. 16 shows the detection probability calculated in ROI 1 for different M values (i.e. different alarm thresholds).

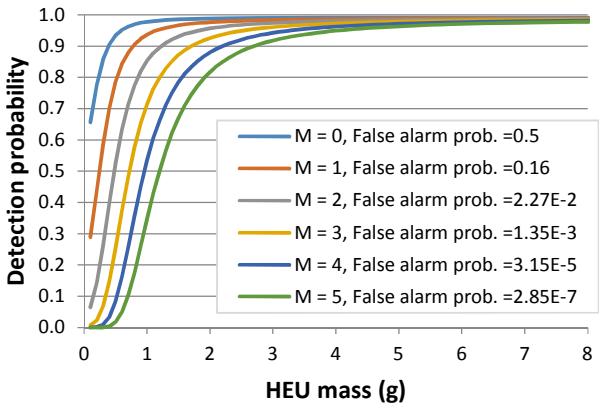

Fig. 16. Detection probability of the tested setup with a bare source of U_3O_8 (HEU).

The detection probability described in Fig. 16 was calculated based on simulation of U_3O_8 (HEU). The variation of auto-absorption with the mass, density or shape was not taken into account to simplify calculations. Fig. 16 is just an approximation of the detection efficiency of the SRPM, small source emit most of their radiations and the real detection efficiency should be better than the calculated one. Additional calculations should be done to take into account the variation of auto-absorption. The detection probabilities calculated in Fig. 16 are nevertheless useful. The detection probability is good for mass above 5g, but for lower mass the threshold alarm has an important impact and the operator must choose between false alarm rate and the SRPM detection efficiency.

III. CONCLUSIONS

Evaluate the performance of a radiation portal monitor is not a simple task. Many scenarios and setups are possible, the environment has an important impact on the results and there are many sources of uncertainties. A combination of experimental data, collected during ITRAP+10 Phase II RRT testing campaign, and simulations is a good way to study the performance of a SRPM in realistic condition. In the paper, the code MCNP6 was used to calculate the detection efficiency of a SRPM. This model showed a good agreement with ITRAP+10 experimental assays. The detection probability was calculated for one source of nuclear material, one shape, and one density but new scenarios must be tested. At the end, the results shall help in the selection of the operating characteristics of the SRPM to choose between false alarm rate and the detection efficiency.

REFERENCES

[1] Ministerial Declaration at the International Conference on Nuclear Security: Enhancing Global Efforts (2013). http://www-pub.iaea.org/MTCD/Meetings/PDFplus/2013/cn203/cn203MinisterialDeclaration.pdf

[2] Incident and Trafficking Database managed by the IAEA. http://www-ns.iaea.org/security/itdb.asp

[3] G. TUDOR, “HEU seizure highlights Moldova’s strong work in nuclear security”, IAEA Division of Public Information (2013).

[4] https://ec.europa.eu/jrc/en/publication/illicit-trafficking-radiation-assessment-program-itrap10-test-campaign-summary-report

[5] C. CARRAPICO, “Illicit Trafficking Radiation Detection Assessment Program ITRAP+10 Phase II Round Robin, Spectroscopic Radiation Portal Monitor, Test Methods”, JRC Technical Reports (2017).

[6] MCNP6, version 1.0., https://mcnp.lanl.gov/

[7] G. F. KNOLL, Radiation Detection and Measurement, 3rd ed. (2000).

[8] Statistique appliquée à l’exploitation des mesures, CETAMA, 2nd edition (1978).

[9] P. E. FEHLAU, “An applications guide to pedestrian special nuclear material monitors”,LA-10633-MS (1986).

[10] D. REILLY, N. ENSSLIN, and H. SMITH, “Passive Nondestructive Assay of Nuclear Materials”, NUREG/CR-5550, Washington, D.C. (1991).